JCTC Journal of Chemical Theory and Computation

Article

pubs.acs.org/JCTC

Adaptive Switching of Interaction Potentials in the Time Domain: An Extended Lagrangian Approach Tailored to Transmute Force Field to QM/MM Simulations and Back

Marcus Böckmann,*[,†] Nikos L. Doltsinis,[†] and Dominik Marx[‡]

[†]Institut für Festkörpertheorie and Center for Multiscale Theory & Computation, Westfälische Wilhelms-Universität Münster, Wilhelm-Klemm-Str. 10, 48149 Münster, Germany

[‡]Lehrstuhl für Theoretische Chemie, Ruhr-Universität Bochum, 44780 Bochum, Germany

ABSTRACT: An extended Lagrangian formalism that allows for a smooth transition between two different descriptions of interactions during a molecular dynamics simulation is presented. This time-adaptive method is particularly useful in the context of multiscale simulation as it provides a sound recipe to switch on demand between different hierarchical levels of theory, for instance between ab initio ("QM") and force field ("MM") descriptions of a given (sub)system in the course of a molecular dynamics simulation. The equations of motion can be integrated straightforwardly using the usual propagators, such as the Verlet algorithm. First test cases include a bath of harmonic oscillators, of which a subset is switched to a different force constant and/or equilibrium position, as well as an all-MM to QM/MM transition in a hydrogen-bonded water dimer. The method is then applied to a smectic 8AB8 liquid crystal and is shown to be able to switch dynamically a preselected 8AB8 molecule from an all−MM to a QM/MM description which involves partition boundaries through covalent bonds. These examples show that the extended Lagrangian approach is not only easy to implement into existing code but that it is also efficient and robust. The technique moreover provides easy access to a conserved energy quantity, also in cases when Nosé−Hoover chain thermostatting is used throughout dynamical switching. A simple quadratic driving potential proves to be sufficient to guarantee a smooth transition whose time scale can be easily tuned by varying the fictitious mass parameter associated with the auxiliary variable used to extend the Lagrangian. The method is general and can be applied to time-adaptive switching on demand between two different levels of theory within the framework of hybrid scale-bridging simulations.

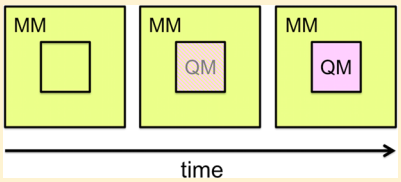

1. INTRODUCTION

Any flavor of the molecular dynamics (MD) simulation method, be it ab initio, force field atomistic, or coarse grained, is applicable only to a limited range of physical or chemical problems. For *any* such method, upper bounds to the treatable system size and time scale are imposed by the computational cost. The suitability of a particular simulation technique for a given problem also crucially depends on whether the approximations made in the method are able to capture the physics and/or chemistry involved. For instance, ab initio simulation techniques being based on a full electronic structure description of the entire system have to be used to gain insight into electronic effects or chemical reactions, whereas force field based MD cannot provide this level of detail.[1]

More importantly, however, for many physical problems, processes occurring on different scales are intimately interlinked, making a treatment with a single simulation method impossible. This realization forms the basis of the research field of multiscale simulation, which aims to combine various existing techniques to access a wider range of systems.[2−13] One of the biggest challenges in simulations across multiple scales is a smooth transition from one representation to another. This problem was first encountered in hybrid quantum mechanics/molecular mechanics (QM/MM) simulations,[2−4] where the total system is divided into fixed partitions that are treated using electronic structure ("QM") and force field ("MM") based descriptions, respectively. Particles initially assigned to the QM partition can at no stage of the simulation become part of the MM partition and vice versa. However, such an adaptive partitioning would be highly desirable in many situations, for instance to allow solvent molecules to switch from an MM to a QM representation if they get sufficiently close to a reactive center or from QM to MM if they diffuse away. The first adaptive QM/MM scheme of this sort was proposed by Rode and co-workers.[14−16] However, their "hot spot" method suffered from force discontinuities and no energy conservation. The former issue was later alleviated by Kerdcharoen and Morokuma,[17] the latter by Heyden et al.,[18] whose sorted adaptive partitioning scheme was subsequently extended by Lin and co-workers.[19,20] Computationally more efficient variants and a density-based partitioning method have subsequently been proposed.[21−23] In a similar spirit, Csányi et al. developed a "learn-on-the-fly" hybrid quantum-classical MD approach,[24] which has been applied to simulate crack propagation in solid materials. Alternative approaches based on an adaptive mesh Ansatz have also been employed in this field.[25−27]

Another class of methods have focused on the transition between an atomistic and a coarse grained force field

Received: February 12, 2015
Published: April 28, 2015

DOI: 10.1021/acs.jctc.5b00142
J. Chem. Theory Comput. 2015, 11, 2429−2439

representation. In this case, the change in the number of degrees of freedom poses additional complications. The "adaptive resolution" approach by Kremer, Delle Site, and co-workers[28−32] uses a force interpolation scheme in the transition region, which fulfills Newton's third law, but does not, however, guarantee energy conservation. Ensing et al.[22,33] devised an alternative force interpolation scheme, which also conserves momentum, but energy conservation is disputed. It stimulated a comment and reply discussion[34,35] on fundamental aspects, such as preserving thermodynamic equilibrium of multiscale switching techniques. A recent state-dependent Hamiltonian formulation[36] alleviates this problem, although fundamental questions remain as to whether energy conservation can be strictly achieved without violating other physical principles.[37]

In the present work, we devise a computational scheme that makes it possible to adaptively "switch on" new interactions while simultaneously "switching off" the old interactions with a focus on transmuting an all-MM simulation dynamically into a QM/MM simulation and vice versa; adaptive partitioning techniques are therefore not the focus of this work. This type of situation is encountered frequently in biomolecular and materials modeling when a time- and space-local change of the QM/MM system, such as a chemical reaction, induces responses that require simulations on extended time and length scales. In the former case, this might be the key chemical reaction in a biochemical signal transduction cascade that induces large-amplitude and thus slow changes in protein complexes.[38,39] In the latter case, photoresponsive materials can be switched by using light which triggers mesoscopic to macroscopic responses which go back to chemical isomerizations of photoswitchable molecules on the angstrom length and femtosecond time-scales.[7,40] In such cases, it would be highly desirable to switch smoothly from a computationally demanding QM/MM propagation scheme to an efficient all-MM simulation after the elementary electronic structure process, i.e., the chemical reaction or the photoswitching process, has terminated. In the reverse all-MM to QM/MM direction, the same idea would allow one within a usual force field simulation to change the representation of a selected subsystem by replacing its force field by an electronic structure description.

The concept of switching from a QM/MM to an all-MM description can also be applied to the computation of absolute free energies of solvation as demonstrated by Gao within the Monte Carlo simulation approach.[41,42] Tuckerman and co-workers have proposed an alchemical adiabatic molecular dynamics method similar in spirit to the approach presented here, which they applied to the calculation of solvation free energies of amino acid switching between two all-MM potentials.[43]

Beyond its use in exchanging the resolution level adaptively on demand in hierarchical hybrid simulations and solvation free energy calculations, our scheme will also be useful in initializing QM/MM simulations. Usually, the only way to realistically prepare the global structure of a complex system is by performing force field simulations from which the initial atomic positions and velocities can be sampled for the subsequent QM/MM run. The switch from the force field to the hybrid QM/MM interactions is normally invoked instantaneously, generally causing discontinuities in the forces on the atoms, with unknown consequences. The scheme presented here will be convenient to smoothly transmute the force field description of a chosen subsystem to its electronic structure treatment.

2. THEORETICAL BACKGROUND

Before we outline the extended Lagrangian approach adopted in this work, let us first mention that it is indeed advantageous compared to a straightforward time-dependent mixing of two potentials V_1 and V_2, with a Lagrangian of the form

$$\mathcal{L} = \frac{1}{2}\sum_{I=1}^{N} M_I \dot{\mathbf{R}}_I^2 - \{a(t)V_1(\mathbf{R}) + [1 - a(t)]V_2(\mathbf{R})\} \tag{1}$$

where $\mathbf{R}$ contains the coordinates $\mathbf{R}_I$ of all N nuclei, and $a(t)$ denotes a function that smoothly varies from 0 to 1 between t_0 and t_1. Using the Euler−Lagrange equation with the Lagrangian defined in eq 1 yields the equation of motion for nucleus I,

$$M_I \ddot{\mathbf{R}}_I = a(t)\mathbf{F}_{1,I} + [1 - a(t)]\mathbf{F}_{2,I} \tag{2}$$

where $\mathbf{F}_{\sigma,I} = -\nabla_I V_\sigma$ is the force on nucleus I from potential V_σ (σ = 1, 2). Unfortunately, this equation of motion cannot be integrated straightforwardly with the popular velocity Verlet algorithm or other standard propagators employed in typical molecular dynamics program packages because its right-hand-side (rhs) is explicitly time-dependent.

Our approach builds instead on an elegant extended Lagrangian approach that has been developed by Tuckerman and co-workers,[43] albeit in a very different context from the present one, namely, to compute solvation free energies via alchemical adiabatic molecular dynamics. Within this approach,[43] a fictitious time-dependent variable $\lambda(t)$ with an associated mass μ is introduced, which allows one to express the total (i.e., mixed) potential as

$$V(\mathbf{R}, \lambda) = g(\lambda)V_1(\mathbf{R}) + h(\lambda)V_2(\mathbf{R}) \tag{3}$$

where the following boundary conditions are imposed on the mixing functions $g(\lambda)$ and $h(\lambda)$

$$g(0) = 1, \quad g(1) = 0, \quad g(\lambda) \in [0, 1] \tag{4}$$

$$h(0) = 0, \quad h(1) = 1, \quad h(\lambda) \in [0, 1] \tag{5}$$

The switch from V_1 to V_2 is achieved by initializing the system with $\lambda = 0$ at $t = 0$ where $g(0) = 1$ and $h(0) = 0$ (thus, the dynamics at $t \leq 0$ is governed exclusively by forces due to V_1) and propagating the system until $\lambda = 1$ is reached, from which moment on it is propagated purely using the forces according to V_2.

Introducing the obvious simplification $h(\lambda) = 1 - g(\lambda)$, the extended Lagrangian[43] becomes

$$\mathcal{L}^{\text{ext}} = \frac{1}{2}\sum_{I=1}^{N} M_I \dot{\mathbf{R}}_I^2 + \frac{1}{2}\mathrm{sgn}(\Delta V)\mu\dot{\lambda}^2 - \{g(\lambda)V_1(\mathbf{R}) + [1 - g(\lambda)]V_2(\mathbf{R})\} \tag{6}$$

where

$$\Delta V \equiv V_1 - V_2 \tag{7}$$

In the second term, we have introduced the sign function to ensure the desired "forward" dynamical evolution of the fictitious particle (see the discussion in section 3.1).

According to the Euler−Lagrange formalism, eq 6 yields the coupled equations of motion

$$M_I \ddot{\mathbf{R}}_I = g(\lambda)\mathbf{F}_{1,I} + (1 - g(\lambda))\mathbf{F}_{2,I} \tag{8}$$

for the nuclei and

DOI: 10.1021/acs.jctc.5b00142
J. Chem. Theory Comput. 2015, 11, 2429−2439

Table 1. Selected Driving Potentials and Forces for Fictitious Variable λ

type	$g(\lambda)$	$F_\lambda = -g'(\lambda)$	$F_\lambda(0)$	$F_\lambda(1)$
linear	$(1 - x)$	+1	1	1
harmonic	$(x - 1)^2$	$-2(x - 1)$	2	0
cubic	$-(x - 1)^3$	$3(x - 1)^2$	3	0
tanh	$1 - \tanh(x\pi)$	$1/\cosh^2(x\pi)$	1	0.01
cosine I	$\cos((\pi/2)x)$	$(\pi/2)\ \sin((\pi/2)\ x)$	0	$(\pi/2)$
cosine II	$(1/2)(1 + \cos(x\pi))$	$(\pi/2)\sin(\pi x)$	0	0
cosine III	$1 + \cos((\pi/2)(x+1))$	$(\pi/2)\sin((\pi/2)(x + 1))$	$(\pi/2)$	0

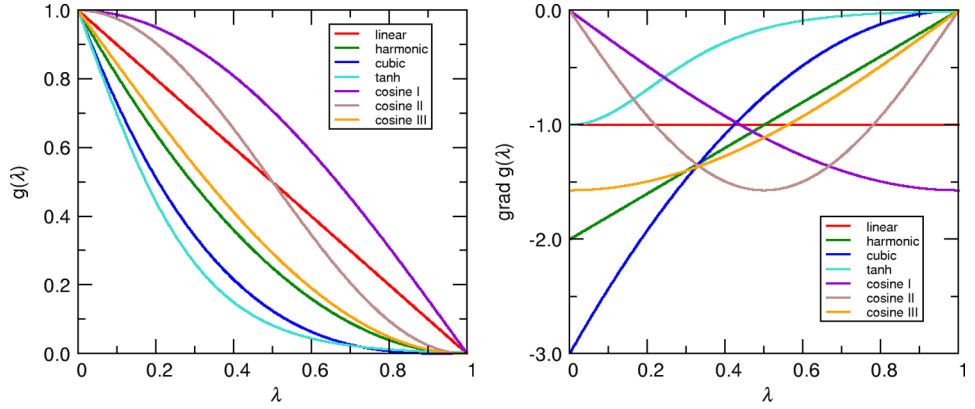

Figure 1. Driving potentials for λ (left) and corresponding derivatives (right) for the set of switching functions compiled in Table 1.

$$\mu\ddot{\lambda} = \mathrm{sgn}(\Delta V)F_\lambda\ \Delta V \tag{9}$$

for the fictitious particle, respectively. The force

$$F_\lambda = -\frac{\mathrm{d}g}{\mathrm{d}\lambda} = -g' \tag{10}$$

on the rhs of eq 9 acts exclusively on the fictitious particle.

It is important to note that—in contrast to eq 2, the rhs's of eq 8 and eq 9 are *not explicitly* time-dependent and hence can be integrated with commonly used numerical methods such as the Verlet algorithm or other standard integrators employed in dynamical simulation packages.

The equations of motion eq 8 and eq 9 can be derived alternatively within the Hamiltonian formalism from the extended Hamiltonian

$$\mathcal{H}^{\mathrm{ext}} = \sum_{I=1}^{N} \frac{\mathbf{P}_I^2}{2M_I} + \mathrm{sgn}(\Delta V)\frac{p_\lambda^2}{2\mu} + \{g(\lambda)V_1(\mathbf{R}) + [1 - g(\lambda)]V_2(\mathbf{R})\} \tag{11}$$

obtained by Legendre transform of the extended Lagrangian given in eq 6. Hamilton's equations yield $\mathbf{P}_I = M_I\ \dot{\mathbf{R}}_I$ and $p_\lambda = \mathrm{sgn}(\Delta V)\mu\dot{\lambda}$ for the nuclear and fictitious momenta, respectively. This leads to the conserved energy

$$E^{\mathrm{cons}} = E^{\mathrm{tot}} + \mathrm{sgn}(\Delta V)E^{\mathrm{kin,\ fict}} \tag{12}$$

where the total energy of the physical system

$$E^{\mathrm{tot}} = \sum_{I=1}^{N} \frac{\mathbf{P}_I^2}{2M_I} + V(\mathbf{R}, \lambda) \tag{13}$$

is the sum of the kinetic energy of the nuclei and the (mixed) potential, eq 3, and

$$E^{\mathrm{kin,\ fict}} = \frac{p_\lambda^2}{2\mu} \tag{14}$$

is the kinetic energy of the fictitious particle. It is noted in passing that having such a conserved quantity at hand during the simulation greatly helps to assess the quality of the simulation.

3. IMPLEMENTATION AND COMPUTATIONAL DETAILS

3.1. Choice of Switching Function $g(\lambda)$. Out of the infinite number of functions $g(\lambda)$ that satisfy the boundary conditions in eq 4 and eq 5, a few relatively simple choices are listed in Table 1 and plotted in Figure 1 together with the corresponding forces F_λ. All of these functions have in common that they give rise to non-negative forces in the switching interval $\lambda \in [0,1]$. To ensure that λ indeed grows from its initial value of 0 to its final value of 1 thereby producing "forward" switching from V_1 to V_2 as desired, the rhs of eq 9 needs to be positive, giving rise to a positive acceleration $\ddot{\lambda}$. While this would be the case naturally for $V_1 > V_2$ even without the sign function, the latter guarantees that this is also true for $V_2 > V_1$. Importantly, the sign function needs to be tracked along the trajectories in order to properly compute the conserved energy according to eq 12.

3.2. Harmonic Oscillators. The method has been tested in detail using a simple model consisting of a large set of identical harmonic oscillators where a subset of n such oscillators were switched to a new force constant and/or a new equilibrium value at a specific moment in time. Using the same numerical implementation in the CPMD program package[44] as for QM/MM switching (see sections 4.2 and 5), the effect of the different switching functions from Table 1 was investigated.

The equations of motion for the harmonic oscillator system of section 4.1 as defined in eq 15 and eq 16 were integrated

DOI: 10.1021/acs.jctc.5b00142
J. Chem. Theory Comput. 2015, 11, 2429−2439

applying the velocity Verlet algorithm with a time step of 0.01 au. The trajectories were, unless stated otherwise, initiated at $x = 1.5$ au with zero velocity, and the initial force constant was set to $k^{(1)} = 5$ au, while the equilibrium position was $x_0^{(1)} = 1.0$ au. The particle masses M_I were set to 1 au. At time t_0, i.e., when the switch was initiated, $x(t_0 = 0) = 0.57525$ au and $v(t_0 = 0) = 0.58984$ au. For the extended Lagrangian switching, a fictitious mass of 5000 au was employed (note that μ has the dimension mass·length^2 as can be easily seen from the extended Lagrangian definition (eq 6)). No thermostat was used when propagating the collection of harmonic oscillators.

3.3. Water Dimer. Next, a small but realistic system, namely, a water dimer in the gas phase, has been switched from a standard force field molecular dynamics simulation (i.e., all-MM) to a QM/MM hybrid simulation where one of the two water molecules is described using full electronic structure theory (see section 4.2. The simulations of the water dimer were carried out using the CPMD program package[44] modified for time-adaptive switching. For the MM description, the flexible SPC water model was used. Standard Gromacs center types (HW and OW) and SPC point charges ($q_O = -0.81$; $q_H = 0.41$) were employed together with the force constant $k_{OH} = 2.32 \times 10^3$ kJ/mol Å^4, the equilibrium distance $r_0 = 1.0$ Å for the OH bonds, the force constant $k_{HOH} = 490$ kJ/mol, and the equilibrium value $a_0 = 104.0°$ for the HOH bond angle. In QM/MM molecular dynamics, which were performed in the Born−Oppenheimer mode (see section 5.5 in ref 1 for a general discussion of dynamical hybrid methods and section 5.5.2.2 for details on the specific interface that is used in the present study), one of the water molecules was treated by density functional theory (DFT) using the BLYP exchange-correlation density functional[45,46] and a plane-wave basis set truncated at 70 Ry in conjunction with employing Troullier-Martins normconserving pseudopotentials. It is noted in passing that this is a standard setup that is often used in typical QM/MM simulations of photochemical and (bio)-molecular reactions; cf. sections 9.13 and 9.14 in ref 1, respectively. Moreover, since the two molecules are connected by a H-bond, it is not required to break a covalent bond when replacing one MM water molecule by a QM molecule; note that the H-bond donating (right) molecule in the following water dimer arrangement, $H_2O\cdots HOH$, is the QM subsystem. The nonperiodic QM box of size $15 \times 15 \times 15$ Å^3 was embedded in a $100 \times 100 \times 100$ Å^3 periodic MM cell. The system was equilibrated at 5 K in this gas phase setup using a Nosé−Hoover[47,48] chain[49,50] thermostat for each degree of freedom and a time step of 5 au. After 40,000 time steps, corresponding to ≈4.8 ps, the switching process was initiated with unchanged thermostatting. On the basis of the findings of the systematic study using the simple harmonic oscillator model, the harmonic driving potential according to Table 1 was applied to induce the all-MM to QM/MM transition in the extended Lagrangian scheme. Different switching speeds were achieved by choosing two different fictitious masses, namely, $\mu = 2.5 \times 10^4$ u a_0^2 and $\mu = 2.5 \times 10^5$ u a_0^2; note that the physical hydrogen mass is 1.008 u and that a_0 is the Bohr radius.

3.4. 8AB8 Liquid Crystal. Finally, the usefulness of the approach in the realm of realistic large-scale QM/MM simulations is demonstrated by switching smoothly a randomly picked molecule in a liquid crystal from MM to QM description, thus transmuting a usual all-MM to a QM/MM hybrid simulation (see 5). The simulations of the smectic 8AB8 liquid crystal were also performed using the CPMD package[44] and closely resemble those of the water dimer at the technical level. What we dubbed the "8AB8 molecule"[51] consists of a photoswitchable azobenzene (AB) functional unit at its center, which is connected symmetrically via two ether bonds to two aliphatic chains containing 8 carbon units each; significant background on the simulation model, a motivation to study it, and references to previous work can be found in a review.[7] The size of the periodic MM unit cell containing 1296 such 8AB8 molecules was $88.1 \times 86.8 \times 131.8$ Å^3, whereas a 18 Å cubic box was used for the nonperiodic QM subsystem. The latter comprises only the azobenzene core of a single 8AB8 molecule together with additional "capping" hydrogen atoms saturating the two "dangling" bonds (cf. section 5.5.2.2 in ref 1) that are generated by cutting the two C−O covalent bonds which connect the two chains via ether bridges (belonging to the MM part) to the AB core (being the QM subsystem). In this case, the QM subsystem was treated using the PBE functional,[52,53] again a 70 Ry plane wave cutoff and Goedecker pseudopotentials. A time step of 20 au was chosen in the Born−Oppenheimer propagation, and the temperature was kept at an average value of 460 K upon applying individual Nosé−Hoover chain thermostats for the MM and QM subsystem, respectively, before, during, and after the switching process. The system was first prepared in the smectic liquid crystalline phase employing coarse grained molecular dynamics and then backmapped onto the all-MM model using a strategy described previously.[7,51] The smooth all-MM → QM/MM switching was again performed by applying the harmonic driving potential with $\mu = 5 \times 10^6$ u a_0^2.

Only in the case of instantaneous switching, which we carried out for reference purposes only, the time step had to be reduced to 5 au in order to ensure numerical stability of the integration scheme. Two sets of all-MM, smoothly switched, and instantaneously switched all-MM → QM/MM simulations were carried out using two different MM force fields. For the first set, the optimized 8AB8 force field (ff1) fitted to DFT reference data as described in detail in ref 51 was employed, whereas the second set was obtained using an artificially perturbed force field (ff2) in which the reference values of the CNNC unit, i.e., NN and CN bond lengths, NNC bond angle, and CNNC and CCNN dihedrals, were increased by 10% compared to those of ff1 and their force constants by 20%.

4. TEST APPLICATIONS

4.1. Bath of Harmonic Oscillators. *4.1.1. Choice of Driving Potential and Fictitious Mass.* The various driving potentials for λ introduced in Table 1 are first tested for a model system of $N = 1000$ identical, uncoupled one-dimensional harmonic oscillators with an initial force constant k_1 and equilibrium position $x_0^{(1)}$. At time $t = 0$, a subset of n oscillators is switched to a new force constant k_2 and/or to another equilibrium position $x_0^{(2)}$. Thus, the initial potential is given by

$$V_1(\mathbf{x}) = \sum_{i=1}^{N} \frac{1}{2} k_1 (x_i - x_0^{(1)})^2 \tag{15}$$

whereas the final potential is

$$V_2(\mathbf{x}) = \sum_{i=1}^{n} \frac{1}{2} k_2 (x_i - x_0^{(2)})^2 + \sum_{i=n+1}^{N} \frac{1}{2} k_1 (x_i - x_0^{(1)})^2 \tag{16}$$

DOI: 10.1021/acs.jctc.5b00142
J. Chem. Theory Comput. 2015, 11, 2429−2439

The top panel of Figure 2 shows the time evolution of $g(\lambda)$ where $\lambda = \lambda(t)$ for the different driving potentials listed in Table 1 when a subset of $n = 100$ oscillators are switched. Our first observation is that for the cos I and cos II functions, $g(\lambda(t))$ remains very close to its initial value of 1.0 (where $\lambda(t = 0) = 0$) for a longer time compared to that of all other switching functions. This is due to the corresponding force F_λ being initially zero for these two choices. In fact, the switching process is not self-starting in this case and had to be triggered by applying a small artificial force. The harmonic, cubic, tanh, and cos III potentials, however, all yield a smooth transition from $\lambda = 0$ to 1 both at the initial *and* final stages of the switching period, whereas the linear potential starts smoothly but finishes abruptly upon reaching $g(1) = 0$. This limits the usefulness of the investigated switching function to the harmonic, cubic, tanh, and cos III forms.

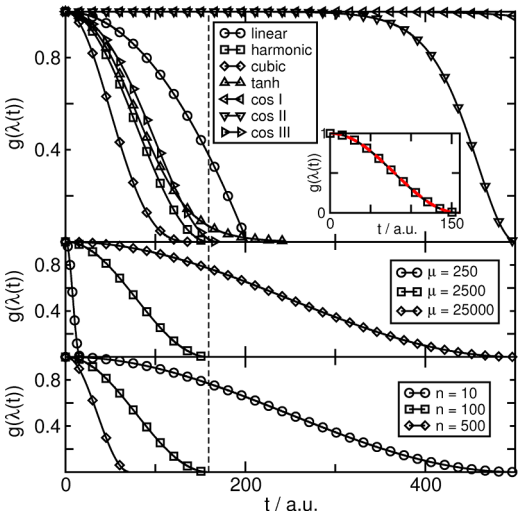

Figure 2. Application of the adaptive switching scheme to a system of 1000 harmonic oscillators with n oscillators switched from $k_1 = 1.0$ au to $k_2 = 1.2$ au at $t_0 = 0$ with $x(t_0) = -0.42915$ au and $v(t_0) = 0.25650$ au. Top: comparison of the time evolution of different driving potentials $g(\lambda(t))$ from Table 1 for $n = 100$ and $\mu = 25000$ au; the inset shows $g(\lambda(t))$ for the harmonic driving potential (open squares) together with the simple cosine function (red solid line) $a(t) = \cos[\pi t/(t_1-t_0)]$, where $t_0 = 0$ and $t_1 = 200$ au; see text. Middle: variation of μ at constant $n = 100$ using the harmonic driving potential. Bottom: variation of n at constant $\mu = 25000$ au using the harmonic driving potential.

Further analysis reveals that, for the harmonic driving potential, the function $g(\lambda(t))$ generated by the underlying switching algorithm corresponds to a simple, *explicitly* time-dependent, mixing function as defined in eq 1 of the form $a(t) = \cos[\pi t/(t_1-t_0)]$, as depicted in the inset of Figure 2 (top panel). We would like to stress, however, that this behavior results from the *propagation* of $\lambda(t)$ according to eq 8 and eq 9 and was not imposed explicitly as it would when using the traditional time-dependent switching Ansatz given by eq 1. For the sake of simplicity, we chose the harmonic driving potential for the tests and applications described below, as it ensures an efficient and smooth switching behavior.

As illustrated in the middle panel of Figure 2, the time span in which the transition takes place is readily tunable by varying the fictitious mass parameter μ. The heavier the fictitious particle, the slower is the switching process and vice versa, in accordance with eq 9. Hence, the fictitious mass parameter μ serves as a control parameter for adjusting the switching time, which also depends on the potential energy net change ΔV in going from V_1 to V_2. In our test system of N harmonic oscillators, ΔV can be conveniently varied by switching different numbers n of oscillators. The effect on the time scale of the transition is demonstrated in the bottom panel of Figure 2, where $g(\lambda(t))$ is plotted for the switching of $n = 10$, 100, and 500 out of a total of 1000 harmonic oscillators. As can be seen from Figure 2 (bottom panel) and expected from eq 9, the switching process speeds up with increasing n, which is equivalent to an increasing ΔV.

The benefit of the smooth Lagrangian (green lines) compared to the instantaneous "brute force" (red) switching, both taking place at $t = 0$, is demonstrated in Figure 3 for the collection of harmonic oscillators (10% of them being switched) compared to the original system (black). The two top row panels show the total energy of the physical system, E^{tot}, as defined in eq 13, in the left panel and the position (right top panel) for a transition in which only the force constant changes ($k_1 = 5$ au, $x_0^{(1)} = 1.0$ au $\rightarrow k_2 = 6$ au, $x_0^{(2)} = 1.0$ au), where V_1 and V_2 are defined according to eq 15 and eq 16. As can be seen, the two switching procedures lead to different energies after the switch. The magnitude of the jump at $t = 0$ for the instantaneous switch can be easily calculated; see below. In the case of the extended Lagrangian, E^{tot} is seen to change smoothly from the value of the original system to that of the totally switched system over a period of about 50 au. The blue line illustrates that the conserved energy, as defined in eq 12, is indeed a numerically constant quantity. Here, it is important to realize that ΔV changes sign repeatedly during the course of the simulation depending on the instantaneous values of V_1 and V_2, which is taken into account at each time step via the corresponding sign term $\mathrm{sgn}(\Delta V)$; see eq 12. The effect of abrupt switching on the oscillation amplitudes is less obvious (see Figure 3, top right panel). However, close inspection of

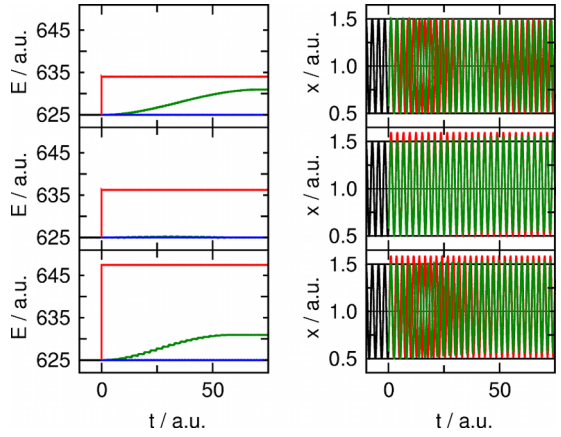

Figure 3. Comparison of smooth (green) versus abrupt (red) switching of 100 out of 1000 (identical) harmonic oscillators to different target potentials starting at $t = 0$, together with the corresponding data for the original system ($t < 0$, black). On the left, the time evolution of the total energy of the physical system (given by eq 13 in the case of smooth switching) is shown. The blue line represents the conserved energy defined via eq 12 for smooth switching. Top row: switch from $k_1 = 5$ au, $x_0^{(1)} = 1.0$ au $\rightarrow k_2 = 6$ au, $x_0^{(2)} = 1.0$ au. Second row: $k_1 = 5$ au, $x_0^{(1)} = 1.0$ au $\rightarrow k_2 = 5$ au, $x_0^{(2)} = 1.05$ au. Bottom row: $k_1 = 5$ au, $x_0^{(1)} = 1.0$ au $\rightarrow k_2 = 6$ au, $x_0^{(2)} = 1.05$ au.

DOI: 10.1021/acs.jctc.5b00142
J. Chem. Theory Comput. 2015, 11, 2429−2439

the data reveals that the smooth switch correctly leads to a slight dampening of the amplitude (to 96% of its initial value after 65.7 au) due to the 20% increase in the force constant, while the instant switch does not.

The middle panels of Figure 3 contain the results for a switch where only the equilibrium position is changed while the force constants are all kept at their original value of 5 au ($k_1 = 5$, $x_0^{(1)} = 1.0$ au $\rightarrow$ $k_2 = 5$ au, $x_0^{(2)} = 1.05$ au). Note that physically this corresponds to *identical* oscillatory motion but with respect to a new reference value x_0. It can be seen that the total energy for the smooth switch is the same before and after the transition and only deviates slightly from the asymptotic value in the intermediate regime (between $t = 0$ and $t \approx 50$ au). This is in contrast to the large jump in energy observed for the abrupt switch, which is accompanied by a nonphysical, sudden increase in the oscillation amplitude by 9% at $t = 0$ (Figure 3 middle right). For the smooth switch, however, the amplitude is unchanged; only the equilibrium position shifts continuously to its new value as expected for this particular change of interactions.

The more general case, where both the force constant and the equilibrium position change ($k_1 = 5$ au, $x_0^{(1)} = 1.0$ au $\rightarrow$ $k_2 = 6$ au, $x_0^{(2)} = 1.05$ au), is depicted in the bottom panels of Figure 3. As expected, the time evolution of the energy and position can be described as a mixture of the two previous, limiting, cases. The jump in E^{tot} for the sudden switch is significantly larger in this case, while the smooth switching procedure yields the same asymptote as that in the top row. The latter again shows that the final value of E^{tot} is solely determined by the change in k and is unaffected by any changes in x_0. After the sudden switch, the amplitude immediately increases by 6%, which is slightly smaller than that in the middle right-hand panel of Figure 3 due to the larger force constant here.

To understand in more depth the discontinuities arising from an instantaneous switch, we carry out the following general analysis. Using the relationships $k_2 = sk_1$ and $x_0^{(2)} = x_0^{(1)} + \Delta x$, the potential energy difference at position **x**, where the switch occurs, can be written as

$$\Delta V(\mathbf{x}) = V_2 - V_1 = \sum_i^n \left[\frac{1}{2} k_1 (s-1)(x_i - x_0^{(1)})^2 - k_1 s \Delta x (x_i - x_0^{(1)}) + \frac{1}{2} k_1 s \Delta x^2 \right] \quad (17)$$

In the following, we set $x_i = x$ for all $i = 1, ..., N$, i.e., all oscillators are initially in phase. In analogy to the three scenarios discussed above in connection with Figure 3, we now distinguish three separate cases: (i) $s = 1$, $\Delta x \neq 0$, the jump in energy becomes

$$\Delta V(x) = nk_1 \left[-(x - x_0^{(1)})\Delta x + \frac{1}{2}\Delta x^2 \right] \quad (18)$$

i.e., the energy difference depends linearly on the switching position x. The only way to perform a smooth switch with $\Delta V = 0$ is at $x = x_0^{(1)} + (1/2)\Delta x$. A graphical representation of eq 18 for $k_1 = 1.0$ au, $\Delta x = 0.05$ au, and $n = 1$ can be seen in Figure 4 (red line). For the example discussed in the middle row of Figure 3 ($x = 0.57525$ au, $x_0^{(1)} = 1.0$ au, $k_1 = 5.0$ au, $n = 100$), eq 18 yields a potential energy difference of $\Delta V = 11.24$ au, which exactly corresponds to the jump observed in the red curve in Figure 3.

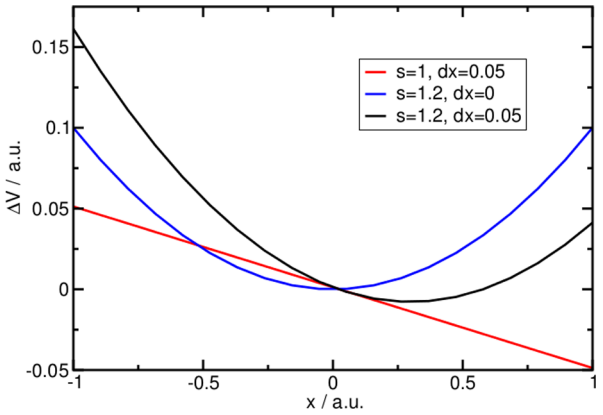

Figure 4. Potential energy difference of the harmonic oscillator system analyzed in Figure 3 due to an instantaneous switch at position x for the three cases (i), (ii), and (iii) defined in the text for $n = 1$, $k_1 = 1.0$ au, and $x_0^{(1)} = 0$: (i) $s = 1$, $\Delta x = 0.05$ au (red line); (ii) $s = 1.2$, $\Delta x = 0$ (blue line); (iii) $s = 1.2$, $\Delta x = 0.05$ au (black line).

(ii) $s \neq 1$ and $\Delta x = 0$: the energy jump

$$\Delta V(x) = \frac{1}{2} nk_1 [(s-1)(x - x_0^{(1)})^2] \quad (19)$$

increases quadratically with displacement x. Hence, a smooth transition is possible only at $x = x^{(0)}$. Equation 19 for $k_1 = 1.0$ au, $s = 1.2$, and $n = 1$ is plotted in Figure 4 (blue line). When we evaluate eq 19 for the example shown in the top row of Figure 3, we obtain an energy shift of $\Delta V = 9.02$ au, explaining quantitatively the discontinuity observed for the abrupt switching procedure seen in Figure 3.

(iii) $s \neq 1$ and $\Delta x \neq 0$: in this general case, the energy difference is

$$\Delta V(x) = \frac{1}{2} nk_1 [(s-1)(x - x_0^{(1)})^2 - 2s(x - x_0^{(1)})\Delta x + s\Delta x^2] \quad (20)$$

which means that there are two switching positions, $x_\pm = x_0^{(1)} + \Delta x s^{1/2} (s^{1/2} \pm 1)/(s-1)$, that do not produce an energy discontinuity. Figure 4 (black line) illustrates eq 20 for $k_1 = 1.0$ au, $s = 1.2$, $\Delta x = 0.05$ au, and $n = 1$. According to eq 20, the energy shift for the case depicted in the bottom panel of Figure 3 is $\Delta V = 22.51$ au, which agrees well with the observation.

4.2. Water Dimer: Switching from All-MM to QM/MM.

As a more realistic test case, we applied our extended Lagrangian method to switch a water dimer in vacuum, $(H_2O)_2$, from a purely molecular mechanics (i.e., all-MM or MM/MM) to a hybrid (QM/MM) representation in which one H_2O molecule is treated with the original water force field (MM) and the other with DFT (QM). Note that, when representing the H-bond arrangement in the water dimer schematically by $H_2O\cdots H^{(1)}O^DH^{(2)}$, it is the right water molecule which donates the H-bond that is represented by DFT after the transmutation.

In Figure 5, we compare two scenarios obtained with the smooth switching method using two different fictitious masses (2.5×10^4 and 2.5×10^5 u a_0^2) to that generated by an instantaneous switch. The unswitched all-MM results are also shown for the sake of comparison. The time evolution of the total energy of the physical system, E^{tot}, shown in Figure 5a, is seen to be smooth for both extended Lagrangian runs, while the instantaneous switch expectedly produces a discontinuity. The

DOI: 10.1021/acs.jctc.5b00142
J. Chem. Theory Comput. 2015, 11, 2429−2439

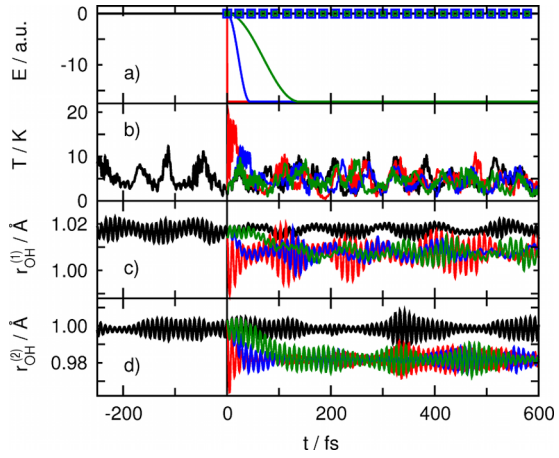

Figure 5. Comparison of smooth Lagrangian versus instantaneous "brute force" all-MM → QM/MM switching for the water dimer, $H_2O\cdots H^{(1)}O^DH^{(2)}$, where the right molecule becomes the QM part after switching. The black lines are the unswitched all-MM reference results, the red lines are for the instantaneous switch, while the blue and green lines are for the extended Lagrangian switch with $\mu = 2.5 \times 10^4$ and $\mu = 2.5 \times 10^5$ u a_0^2, respectively. (a) Total energy E^{tot} of the physical system given by eq 13 and conserved energy E^{cons} corresponding to eq 12 for $\mu = 2.5 \times 10^4$ u a_0^2 (blue line and squares, respectively) and $\mu = 2.5 \times 10^5$ u a_0^2 (green line and circles, respectively), respectively. Note that all energies plotted here include the proper contributions from the fictitious degrees of freedom due to Nosé−Hoover thermostatting and that the green circles are partially inscribed in the blue squares due to the nearly perfect overlay of the data. (b) Temperature of the nuclear subsystem. (c) Covalent $O^DH^{(1)}$ bond length involving the proton that donates the H-bond. (d) Covalent $O^DH^{(2)}$ bond length not involved in H-bonding.

lighter fictitious mass of 2.5×10^5 u a_0^2 (blue line) leads to a more rapid transmutation from the all-MM to the QM/MM representation of the interactions in the case of continuous switching. Also shown in Figure 5a is the conserved energy, eq 12, for the two fictitious masses. Apart from minor deviations arising in the transition region, this conserved quantity is seen to be constant throughout the MD propagation and to follow closely the total energy of the unswitched reference system. We would like to point out that all energies discussed in this section include the contributions from the fictitious degrees of freedom of the Nosé−Hoover thermostat employed in the simulation.

A large jump in temperature of the molecular system close to $t = 0$ with subsequent significant perturbations of the fluctuations can be seen for the instantaneous switch in panel b of Figure 5, whereas the temperature fluctuations of both smoothly switched trajectories feature a behavior that is qualitatively indistinguishable from the original system that has been propagated beyond $t = 0$.

The effect of the switching procedure on the molecular motion is exemplified in Figure 5c and d for the two covalent OH bond lengths of the H_2O molecule that undergoes the transition from a MM to a QM representation. Recall that no covalent bond must be cut across the QM/MM boundary but just an H-bond, which is parametrized in most force fields (such as the flexible SPC water model used herein) in terms of the usual nonbonded interactions which include electrostatics. It is noted in passing that rigid-body constraints at the level of the force field description, e.g., when using rigid water models as often done in biomolecular simulations, would impose additional complications in the switching procedure. A straightforward workaround would be to change from rigid-body to fully flexible MM propagation (or vice versa) before switching from MM to QM/MM molecular dynamics (or vice versa). Clearly, the instantaneous switching protocol induces a large perturbation in both OH bond length vibrations, which is due to a slight mismatch of the equilibrium bond lengths in the two representations. In particular, panel c reveals a nonphysical increase of the fluctuation amplitude of the $O^DH^{(1)}$ bond motion for quite some time after the "brute force" switch, which exceeds that of the unperturbed original system (that has been propagated beyond $t = 0$ for reference) by far. Thus, the covalent bond of the QM molecule that establishes the H-bond to the MM water molecule is strongly perturbed for several oscillation periods after abrupt switching. This $O^DH^{(1)}$ bond is slightly longer than the dangling (free) $O^DH^{(2)}$ bond (compare panel c to d in Figure 5). The former changes from an equilibrium value of about 1.02 Å in the MM model to ca. 1.01 Å in the QM treatment, while the latter shifts from 1.00 Å (MM) to 0.98 Å (QM). Since the vibrational frequencies are also slightly different in the two potentials, we have a scenario comparable to case iii in the harmonic oscillator model presented above, cf. eq 20. However, the energy jump induced by the instantaneous switch is negligible in this case because the displacement from equilibrium was very small at the time of the switch due to the very low simulation temperature of 5 K. It is apparent from Figure 5c and d that the extended Lagrangian switching procedure leads to a smooth shift of the equilibrium OH distance and, at the same time, does not lead to an artificial increase of the amplitude of the bond length fluctuations as observed as a result of instantaneous switching. In general, the more abruptly the switch is performed the larger the vibrational amplitudes after the transition.

5. TIME-ADAPTIVE SWITCHING IN A LIQUID CRYSTAL

Finally, the extended Lagrangian switching method was applied to a liquid crystalline 8AB8 system in which one molecule should undergo a transition from a purely MM to a QM/MM description (see Figure 6). It is noted in passing that the following time-adaptive switching procedure, i.e., all-MM to QM/MM transmutation and back, can be applied repeatedly by selecting stochastically, one after another, the QM molecule subject to photoisomerization.

In significant contrast to the water dimer discussed above, the boundary between the QM and MM partitions now cuts through two covalent bonds as explained in detail in section 3.4, potentially rendering this system more susceptible to perturbations induced by the MM/MM to QM/MM transition. To test the robustness of our smooth switching method, we carried out two sets of simulations with different force fields, the optimized force field ff1 and the perturbed force field ff2 (see section 3.4). Figure 7 compares the time evolution of the total energy of the physical system, E^{tot}, for the time-adaptive and instantaneous switching procedures obtained with the optimized force field ff1 (top panel) and the perturbed force field ff2 (bottom panel). It should be noted that all energies discussed here contain contributions from the fictitious degrees of freedom of the Nosé−Hoover thermostat employed. This total energy E^{tot} smoothly connects both hierarchical levels of description during adaptive switching. Figure 7 also illustrates that the conserved energy, E^{cons} (cf. eq 12), is indeed constant throughout the entire trajectory, i.e., at the onset and after completing the switching process which includes continuous thermostatting. It, moreover, lies on top of the total energy of

DOI: 10.1021/acs.jctc.5b00142
J. Chem. Theory Comput. 2015, 11, 2429−2439

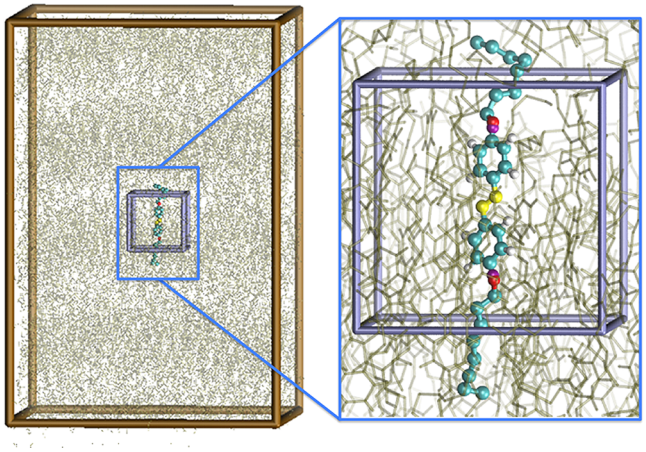

Figure 6. Left: Snapshot of the simulated liquid crystalline 8AB8 system (the layering due to its smectic order gives rise to the vertical periodic density variations) in its periodic MM unit cell with the nonperiodic QM unit cell inside. Right: Magnification of the QM box wherein the particular 8AB8 molecule that is time-adaptively switched from an MM/MM to a QM/MM description is highlighted in a colored ball-and-stick representation together with the QM unit cell. The QM part of the molecule is the azobenzene core ($-C_6H_4-N{=}N-C_6H_4-$) saturated by capping hydrogens (purple balls), which is connected via an ether bridge (red balls) on both termini to the C_8-alkyl chains in the united-atom representation.

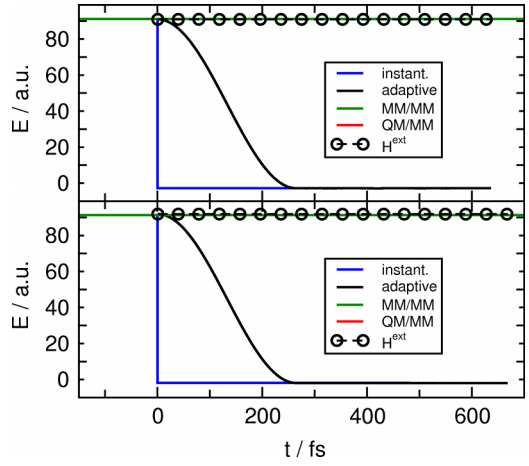

Figure 7. Energy contributions as a function of time for the 8AB8 liquid crystal during an all-MM → QM/MM transition using the extended Lagrangian method with a harmonic switching potential and a fictitious mass of 5×10^6 u a_0^2. The top panel shows data for the optimized force field (ff1), whereas the bottom panel contains data for the perturbed force field (ff2) as described in section 3.4. The total energy of the physical system, E^{tot}, according to eq 13 in the case of the extended Lagrangian trajectory (red line) smoothly connects the value for the unswitched all-MM reference system (green line) at $t = 0$ with that for the QM/MM system at $t \approx 250$ fs, whereas the instantaneously switched trajectory (blue line) shows a large discontinuity at $t = 0$. The conserved energy, E^{cons}, corresponding to eq 12 (black circles), is indeed constant after the time-adaptive switching sets in and follows the total energy of the unswitched system that has been continued to provide the reference for the conserved energy. Note that all energies plotted here include the usual contributions from the fictitious degrees of freedom due to Nosé–Hoover thermostatting.

the unswitched MM reference curve as it should. Addressing now the instantaneous switching curve, it should be noted that a stable propagation could only be obtained after decreasing the MD time step of 5 au, which is four times smaller than the one used in the adaptive simulation. This reduction was necessary because both the regular time step of 20 au and even a reduced time step of 10 au led to program failure due to numerical instabilities in the "brute force" approach. We would like to stress that the advantageous properties of the extended Lagrangian method observed above are independent of whether ff1 or ff2 was used, i.e., the approach is not sensitive to the quality of the match between the MM and QM potential.

We have also performed a detailed analysis of how different switching procedures affect molecular motion. In the case of force field ff1, the changes induced by the transition in most bond lengths, bond angles, and dihedrals monitored are not clearly distinguishable from the fluctuations occurring naturally, even for the abrupt switch. The reason for this is that this particular azobenzene force field has been carefully parametrized against the corresponding DFT data,[51] and therefore, differences in the MM and QM interactions and thus in the potential energies V_1 and V_2 are rather small by construction. One of the biggest effects is visible in the oscillations of the two covalent C–O bonds (see Figure 8) through which the QM/MM boundary runs in order to couple the phenyl rings of the azobenzene moiety (QM) to the two aliphatic chains (which are already part of the MM system together with all other 8AB8 molecules in the liquid crystal) via ether linkages. In the upper and lower panels of Figure 8, the bond length oscillations of these two C–O bonds ("upper" and "lower", respectively; cf. Figure 6) are plotted against time. While the adaptive switching method clearly produces a smooth continuation of the MM curve from $t = 0$ onward, the instantaneous switch causes a noticeable increase in the amplitude of the oscillatory motion of the C–O bond shown in the upper panel. This can be understood in terms of the detailed harmonic oscillator analysis presented in section 4.1. At the time of the switch, the respective upper C–O bond turned out to be stretched to about 1.39 Å, which is far from its equilibrium distance

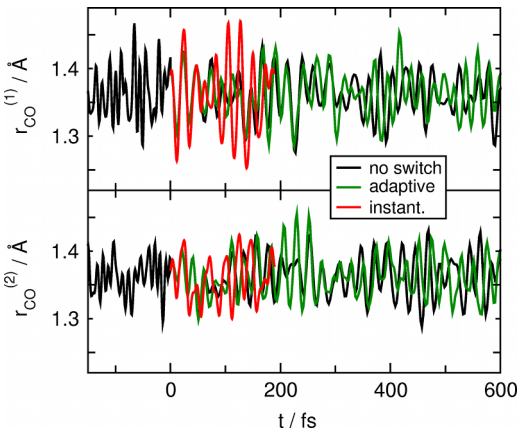

Figure 8. Time evolution of the lengths of the two covalent C–O bonds through which the QM/MM interface cuts in the switched 8AB8 molecule, being part of the smectic liquid crystal, during an all-MM → QM/MM transition (upper panel, $r_{CO}^{(1)}$; lower panel, $r_{CO}^{(2)}$). The green curve was obtained with the adaptive extended Lagrangian method using the harmonic switching potential and a fictitious mass of 5×10^6 u a_0^2, while the red curve is for instantaneous ("brute force") switching. For comparison, the continued unswitched all-MM trajectory is also shown in black.

DOI: 10.1021/acs.jctc.5b00142
J. Chem. Theory Comput. 2015, 11, 2429–2439

(corresponding to $\Delta x \approx 0.03$ Å in eq 20), whereas the other, lower C−O bond happens accidentally to be near equilibrium ($\Delta x \approx 0$) at abrupt switching. Thus, "brute force" switching can easily lead to significant local perturbations in the dynamics, depending on the specific configuration at the time of switching, which can easily propagate in the molecular system due to phenomena such as artificial heat flow and steric clashes.

This effect is considerably magnified when the MM force field deviates more strongly from the QM potential as is the case for ff2. Figures 9 and 10 illustrate the perturbations

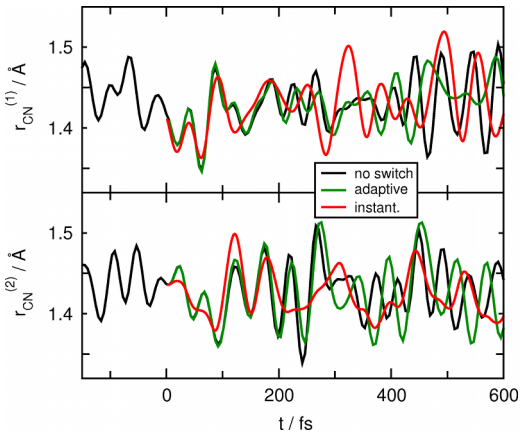

Figure 9. Time evolution of the lengths of the two covalent C−N bonds in the switched 8AB8 molecule during an all-MM → QM/MM transition with the optimized force field ff1 (upper panel, $r_{CN}^{(1)}$; lower panel, $r_{CN}^{(2)}$). The green curve was obtained with the adaptive extended Lagrangian method using the harmonic switching potential and a fictitious mass of 5×10^6 u a_0^2, while the red curve is for instantaneous ("brute force") switching. For comparison, the continued unswitched all-MM trajectory is also shown in black.

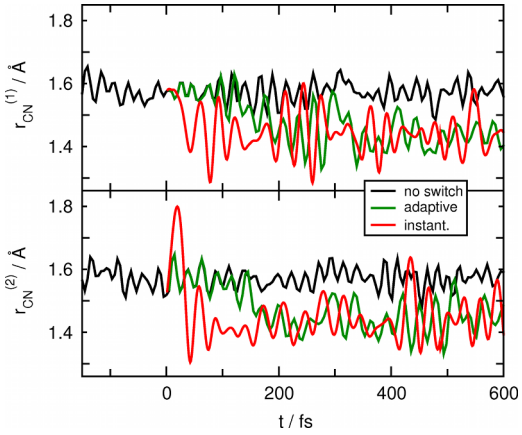

Figure 10. Time evolution of the lengths of the two covalent C−N bonds in the switched 8AB8 molecule during an all-MM → QM/MM transition with the perturbed force field ff2 (upper panel, $r_{CN}^{(1)}$; lower panel, $r_{CN}^{(2)}$). The green curve was obtained with the adaptive extended Lagrangian method using the harmonic switching potential and a fictitious mass of 5×10^6 u a_0^2, while the red curve is for instantaneous ("brute force") switching. For comparison, the continued unswitched all-MM trajectory is also shown in black.

induced by instantaneous switching on the two C−N bond lengths of the selected 8AB8 molecule with ff1 and ff2, respectively. While there are no significant differences in the fluctuations with the optimized force field ff1 (Figure 9), abrupt switching with the perturbed force field ff2 leads to much larger amplitude oscillations than smooth switching (Figure 10).

Last but not least, we do not see any problems in applying our method to QM/MM simulations of other, even more complex systems. As far as the choice of the analytical form of the switching function is concerned, we have shown that the simple harmonic switching function is sufficient in practice. The precise choice of the fictitious mass depends, for any specific application, on the switching time scale desired by the user in conjunction with the difference between the two representations that are coupled by the adaptive switching process, as explicitly demonstrated by using the simple harmonic oscillator test system. As usual when extended Lagrangian methods are employed, the numerical value of the fictitious mass parameter must be validated for each specific application, but the choices provided here for the two molecular systems should be good estimates to start with.

6. CONCLUSIONS AND OUTLOOK

We have presented an extended Lagrangian formalism that allows for a smooth transition in the time domain between two different interaction potentials during a molecular dynamics simulation. The method is useful in the context of multiscale simulation as it provides a sound recipe to connect different hierarchical levels of theory, for instance, ab initio (QM) and force field (MM) molecular dynamics in the spirit of hybrid (QM/MM) molecular dynamics. In particular, a force field simulation can be dynamically transmuted on demand into a hybrid simulation upon changing the MM treatment of a typically small "hot spot" part of a large system into a QM subsystem and vice versa. Similarly, it is also possible to exchange the interaction potentials of the entire system between two preselected levels.

As a first test case, we studied a collection of harmonic oscillators, of which a subset was switched to a potential with different force constant and/or equilibrium position. This toy model showed that a simple quadratic driving potential is sufficient to guarantee a smooth transition and that the time scale of the switch can be easily tuned by adjusting the mass of the fictitious variable that is associated with the auxiliary degree of freedom. Furthermore, this simple system allowed us to demonstrate that abrupt "brute force" switching does not conserve energy, whereas the conserved energy associated with the extended Lagrangian is perfectly constant throughout the propagation including the switching phase. Useful analytical expressions for the jump in energy in the case of abrupt switching could be worked out for the harmonic toy model to make clear that this discontinuity depends on the particular configuration at switching and, thus, is difficult to predict and to control in the case of realistic simulations.

In a more realistic second test, a water dimer in vacuum was switched from an all−MM to a QM/MM representation. It could be shown that instantaneous switching induces severe perturbations in the system with regard to temperature fluctuations and covalent bond dynamics, which are absent in our smooth switching simulations. For this system, thermostatting via Nosé−Hoover chains has been used not only to set the temperature but in particular to ensure proper equipartition of kinetic energy in a small system with stiff covalent bonds that are essentially dynamically decoupled from softer intermolecular interactions. Our time-adaptive switching formalism is shown to yield a numerically constant conserved energy which

DOI: 10.1021/acs.jctc.5b00142
J. Chem. Theory Comput. 2015, 11, 2429−2439

is identical to that before dynamical switching sets in, i.e., to the all-MM value.

Our final application was the transmutation of a force field description of a smectic 8AB8 liquid crystal into one where a single azobenzene photoswitch is represented by its full electronic structure. Here, smooth switching from all-MM to QM/MM interactions proved crucial in order to maintain the same (large) time step in both all-MM and QM/MM simulations. In contrast, instantaneous switching led to numerical failures unless the time step was significantly decreased. Moreover, even for the present case where the force field has been carefully matched to the corresponding QM description, perturbations in the oscillatory dynamics of certain bonds could be detected after switching abruptly, depending accidentally on the magnitude of their displacement from equilibrium at the time of the transition in agreement with the analysis of the harmonic oscillator model. Such perturbation can propagate for long times and over large distances through the switched system via heat flow and steric interaction mechanisms. Again, energy is conserved before, during, and after time-adaptive switching including continuous Nosé–Hoover chain thermostatting.

We conclude that the current time-adaptive approach constitutes an efficient and robust way of smoothly switching from one interaction potential to another one during a molecular dynamics simulation. Implementation is straightforward in as far as the usual propagators, such as the Verlet algorithm, can be used to solve the equations of motion. This approach opens up an efficient way to dynamically switch on and off chemical resolution in terms of an electronic structure description of a typically small subsystem, a "hot spot," that is embedded in a large environment acting as a chemically inert but structurally responsive matrix. Such a procedure is most welcome when studying the impact of chemical reactions or photoswitching processes, which require an electronic structure representation, where changing from a standard force field simulation to QM/MM molecular dynamics allows one to locally zoom in and out on demand. Last but not least, it is stressed that the key idea is by no means restricted to switching forth and back between atomistic force field and QM/MM simulations but that it can be extended to coarse grained force fields as well.

AUTHOR INFORMATION

Corresponding Author

*E-mail: marcus.boeckmann@uni-muenster.de.

Funding

The research has been carried out in the framework of the multi-node joint project 'Adaptive Multiscale Simulation: Connecting the Quantum to the Mesoscopic Level' that has been funded by the Volkswagen Foundation and the simulations have been carried out on JUROPA at NIC Jülich.

Notes

The authors declare no competing financial interest.

ACKNOWLEDGMENTS

We are particularly grateful to Mark Tuckerman for having pointed out to us his general extended Lagrangian Ansatz that underlies our present work as well as to Biswaroop Mukherje and Christine Peter for providing us with equilibrated all-MM configurations that have been backmapped from their coarse grain simulations. Moreover, Kurt Kremer and Luigi Delle Site are kindly acknowledged for fruitful discussions on adaptive computer simulations.

REFERENCES

(1) Marx, D., Hutter, J. *Ab Initio Molecular Dynamics: Basic Theory and Advanced Methods*; Cambridge University Press: Cambridge, 2009.
(2) Warshel, A.; Levitt, M. *J. Mol. Biol.* **1976**, *103*, 227–249.
(3) Gao, J. In *Reviews in Computational Chemistry*; Lipkowitz, K. B., Boyd, D. B., Eds.; VCH: New York, 1995; Vol. 7; pp 119–185.
(4) Senn, H. M.; Thiel, W. *Angew. Chem., Int. Ed.* **2009**, *48*, 1198–1229.
(5) Grotendorst, J., Attig, N., Blügel, S., Marx, D., Eds. *Multiscale Simulation Methods in Molecular Sciences*; Forschungszentrum Jülich: Jülich, Germany, 2009.
(6) Poma, A. B.; Delle Site, L. *Phys. Rev. Lett.* **2010**, *104*, 250201-1–250201-4.
(7) Böckmann, M.; Marx, D.; Peter, C.; Delle Site, L.; Kremer, K.; Doltsinis, N. L. *Phys. Chem. Chem. Phys.* **2011**, *13*, 7604–7621.
(8) Grotendorst, J., Sutmann, G., Gompper, G., Marx, D., Eds. *Hierarchial Methods for Dynamics in Complex Molecular Systems*; Forschungszentrum Jülich: Jülich, Germany, 2012.
(9) Wassenaar, T. A.; Ingolfsson, H. I.; Prieß, M.; Marrink, S. J.; Schäfer, L. V. *J. Phys. Chem. B* **2013**, *117*, 3516–3530.
(10) Karplus, M. *Angew. Chem., Int. Ed.* **2014**, *53*, 9992–10005.
(11) Kalli, A. C.; Sansom, M. S. P. *Biochem. Soc. Trans.* **2014**, *42*, 1418–1424.
(12) Potestio, R.; Peter, C.; Kremer, K. *Entropy* **2014**, *16*, 4199–4245.
(13) Delle Site, L. *Entropy* **2014**, *16*, 23–40.
(14) Kerdcharoen, T.; Liedl, K. R.; Rode, B. M. *Chem. Phys.* **1996**, *211*, 313–323.
(15) Schwenk, C. F.; Loeffler, H. H.; Rode, B. M. *J. Am. Chem. Soc.* **2003**, *125*, 1618–1624.
(16) Hofer, T. S.; Pribil, A. B.; Randolf, B. R.; Rode, B. M. *J. Am. Chem. Soc.* **2005**, *127*, 14231–14238.
(17) Kerdcharoen, T.; Morokuma, K. *Chem. Phys. Lett.* **2002**, *355*, 257–262.
(18) Heyden, A.; Lin, H.; Truhlar, D. G. *J. Phys. Chem. B* **2007**, *111*, 2231–2241.
(19) Pezeshki, S.; Lin, H. *J. Chem. Theory Comput.* **2011**, *7*, 3625–3634.
(20) Pezeshki, S.; Davis, C.; Heyden, A.; Lin, H. *J. Chem. Theory Comput.* **2014**, *10*, 4765–4776.
(21) Bulo, R. E.; Ensing, B.; Sikkema, J.; Visscher, L. *J. Chem. Theory Comput.* **2009**, *5*, 2212–2221.
(22) Nielsen, S. O.; Moore, P. B.; Ensing, B. *Phys. Rev. Lett.* **2010**, *105*, 237802–1–237802–4.
(23) Waller, M. P.; Kumbhar, S.; Yang, J. *ChemPhysChem* **2014**, *15*, 3218–3225.
(24) Csányi, G.; Albaret, T.; Payne, M.; De Vita, A. *Phys. Rev. Lett.* **2004**, *93*, 175503–1–175503–4.
(25) Rafii-Tabar, H.; Hua, L.; Cross, M. *J. Phys. Cond. Mater.* **1998**, *10*, 2375–2387.
(26) Smirnova, J. A.; Zhigilei, L. V.; Garrison, B. J. *Comput. Phys. Commun.* **1999**, *118*, 11–16.
(27) Broughton, J. Q.; Abraham, F. F.; Bernstein, N.; Kaxiras, E. *Phys. Rev. B* **1999**, *60*, 2391–2403.
(28) Praprotnik, M.; Delle Site, L.; Kremer, K. *J. Chem. Phys.* **2005**, *132*, 224106-1–224106-17.
(29) Wang, H.; Schütte, C.; Delle Site, L. *J. Chem. Theory Comput.* **2012**, *8*, 2878–2887.
(30) Fritsch, S.; Poblete, S.; Junghans, C.; Ciccotti, G.; Delle Site, L.; Kremer, K. *Phys. Rev. Lett.* **2012**, *108*, 170602-1–170602-5.
(31) Wang, H.; Hartmann, C.; Schütte, C.; Delle Site, L. *Phys. Rev. X* **2013**, *3*, 011018-1–011018-16.
(32) Agarwal, A.; Wang, H.; Schütte, C.; Delle Site, L. *J. Chem. Phys.* **2014**, *141*, 034102-1–034102-12.
(33) Ensing, B.; Nielsen, S. O.; Moore, P. B.; Klein, M. L.; Parrinello, M. *J. Chem. Theory Comput.* **2007**, *3*, 1100–1105.

DOI: 10.1021/acs.jctc.5b00142
J. Chem. Theory Comput. 2015, 11, 2429–2439

(34) Praprotnik, M.; Poblete, S.; Delle Site, L.; Kremer, K. *Phys. Rev. Lett.* **2011**, *107*, 099801-1−099801-2.
(35) Nielsen, S. O.; Moore, P. B.; Ensing, B. *Phys. Rev. Lett.* **2011**, *107*, 099802.
(36) Potestio, R.; Fritsch, S.; Español, P.; Delgado-Buscalioni, R.; Kremer, K.; Everaers, R.; Donadio, D. *Phys. Rev. Lett.* **2013**, *110*, 108301-1−108301-5.
(37) Delle Site, L. *Phys. Rev. E* **2007**, *76*, 047701-1−047701-4.
(38) Grossfield, A. *Biochim. Biophys. Acta* **2011**, *1808*, 1868−1878.
(39) Johnston, J. M.; Filizola, M. *Curr. Opin. Struct. Biol.* **2011**, *21*, 552−558.
(40) Feringa, B. L., Browne, R. W., Eds. *Molecular Switches*; Wiley-VCH: Weinheim, Germany, 2011.
(41) Gao, J. *J. Phys. Chem.* **1992**, *96*, 537−540.
(42) Gao, J.; Xia, X. *Science* **1992**, *258*, 631−635.
(43) Abrams, J. B.; Rosso, L.; Tuckerman, M. E. *J. Chem. Phys.* **2006**, *125*, 074115−1−074115−12.
(44) Hutter, J. et al. Car-Parrinello Molecular Dynamics: An *Ab Initio* Electronic Structure and Molecular Dynamics Program. www.cpmd.org, (accessed Aug 2014) .
(45) Becke, A. D. *Phys. Rev. A* **1988**, *38*, 3098−3100.
(46) Lee, C.; Yang, W.; Parr, R. C. *Phys. Rev. B* **1988**, *37*, 785−789.
(47) Nosé, S. *J. Chem. Phys.* **1984**, *81*, 511−519.
(48) Hoover, W. G. *Phys. Rev. A* **1985**, *31*, 1695−1697.
(49) Martyna, G. J.; Klein, M. L.; Tuckerman, M. E. *J. Chem. Phys.* **2002**, *97*, 2635−2643.
(50) Tuckerman, M. E. *Statistical Mechanics: Theory and Molecular Simulation*; Oxford University Press: New York, 2010.
(51) Böckmann, M.; Peter, C.; Delle Site, L.; Doltsinis, N. L.; Kremer, K.; Marx, D. *J. Chem. Theory Comput.* **2007**, *3*, 1789−1802.
(52) Perdew, J. P.; Burke, K.; Ernzerhof, M. *Phys. Rev. Lett.* **1996**, *77*, 3865−3868.
(53) Perdew, J. P.; Burke, K.; Ernzerhof, M. *Phys. Rev. Lett.* **1997**, *78*, 1396.

DOI: 10.1021/acs.jctc.5b00142
J. Chem. Theory Comput. 2015, 11, 2429−2439